Article type : Research Article

Quantification of the geometric uncertainty when using implanted markers as a surrogate for lung tumor motion

Nicholas Hardcastle*[4,5], Adam Briggs*[1], Vincent Caillet[1,3], Giorgios Angelis[1,2], Danielle Chrystall[1], Dasantha Jayamanne[1,6], Meegan Shepherd[1], Ben Harris[7], Carol Haddad[1], Thomas Eade[1,6], Paul Keall[3] and Jeremy Booth[1,2]

[1]Northern Sydney Cancer Centre, Level 1 Royal North Shore Hospital, Reserve Rd St Leonards NSW 2065

[2]School of Physics, University of Sydney, Camperdown NSW 2042

[3]ACRF Image X Institute, School of Medicine, University of Sydney, Camperdown NSW 2006

[4]Peter MacCallum Cancer Centre, Melbourne, VIC, 3000

[5]Centre for Medical Radiation Physics, University of Wollongong, Wollongong, NSW, 2522

[6]School of Medicine, University of Sydney Camperdown NSW 2042

[7]Dept Respiratory and sleep Medicine, Level 8 Royal North Shore Hospital, Reserve Rd, St Leonards NSW 2065

*authors contributed equally to this work

Corresponding author:

Dr. Nicholas Hardcastle

Physical Sciences

Peter MacCallum Cancer Centre

Melbourne, VIC, 3000

Australia

This article has been accepted for publication and undergone full peer review but has not been through the copyediting, typesetting, pagination and proofreading process, which may lead to differences between this version and the Version of Record. Please cite this article as doi: 10.1002/MP.14788

Nick.hardcastle@petermac.org

Short title: Surrogacy uncertainty of lung transponders

Acknowledgements:

The authors thank the patients who enrolled in the LIGHT SABR clinical trial and the team of people involved in acquiring the large amount of data used in the present study. JTB acknowledges support for LIGHT SABR clinical study by a Varian Medical Systems Collaborative Research Grant.

Conflict of interest:

NH is supported by a Varian Medical Systems Collaborative Research Grant for an unrelated project. PJK is an inventor on the awarded US patents 7,469,035 and 8,971,489 that are related to MLC tracking. Patent #7,469,035 is unlicensed, patent #8,971,489 has been licensed by the University of Sydney to Leo Cancer Care. JTB (Royal North Shore Hospital) is supported by a Varian Medical Systems Collaborative Research Grant. PJK is supported by an NHMRC Senior Principal Research Fellowship.

Sources of Funding: Varian Medical Systems partially supported this study

Author contributions:

NH and AB conceived of the study, performed data analysis and wrote the manuscript. VC assisted with data collection and analysis. GA and DC performed data analysis and manuscript preparation. DJ, CH, TE recruited patients and provided clinical assessment of collected data. MS assisted with data collection and analysis. BH performed marker insertion. PK and JB conceived of the study and assisted with data interpretation and manuscript preparation

Abstract

Background

Fiducial markers are used as surrogates for tumor location during radiation therapy treatment. Developments in lung fiducial marker and implantation technology has provided a means to insert markers endobronchially for tracking of lung tumors. This study quantifies the surrogacy uncertainty (SU) when using endobronchially implanted markers as a surrogate for lung tumor position.

Methods

We evaluated SU for 17 patients treated in a prospective electromagnetic guided MLC tracking trial. Tumor and markers were segmented on all phases of treatment planning 4DCTs and all frames of pre-treatment kilovoltage fluoroscopy acquired from lateral and frontal views. The difference in tumor and marker position relative to end-exhale position was calculated as the SU for both imaging methods and the distributions of uncertainties analyzed.

Results

The mean (range) tumor motion amplitude in the 4DCT scan was 5.9 mm (1.7 – 11.7 mm) in the superior-inferior (SI) direction, 2.2 mm (0.9 – 5.5 mm) in the left-right (LR) direction, and 3.9 mm (1.2 – 12.9 mm) in the anterior-posterior (AP) direction. Population based analysis indicated symmetric SU centered close to 0 mm, with maximum 5^{th}/95^{th} percentile values over all axes of -2.0 mm/2.1 mm with 4DCT, and -2.3/1.3 mm for fluoroscopy. There was poor correlation between the SU measured with 4DCT and that measured with fluoroscopy on a per-patient basis. We observed increasing SU with increasing surrogate motion. Based on fluoroscopy analysis, the mean (95% CI) SU was 5% (2% – 8%) of the motion magnitude in the SI direction, 16% (6% – 26%) of the motion magnitude in the LR direction, and 33% (23% – 42%) of the motion magnitude in the AP direction. There was no dependence of SU on marker distance from the tumor.

Conclusion

We have quantified SU due to use of implanted markers as surrogates for lung tumor motion. Population 95^{th} percentile range are up to 2.3 mm, indicating the approximate contribution of SU to total geometric uncertainty. SU was relatively small compared with the SI motion, but substantial compared with LR and AP motion. Due to uncertainty in estimations of patient-specific SU, it is recommended that population-based margins are used to account for this component of the total geometric uncertainty.

Key words: stereotactic ablative body radiotherapy, fiducial, lung cancer, stereotactic body radiation therapy, respiratory motion

Introduction

Accurate targeting of treatment volumes in radiation therapy requires identification of the location of the target relative to the treatment machine coordinate system. In general this is achieved using image guidance, in which images are acquired immediately prior and/or during the treatment session, and the patient position is adjusted to ensure the target volume is correctly positioned [1]. This may be supplemented by the use of implanted fiducial markers, which can act as a surrogate for soft-tissue targets not otherwise visualized with planar imaging [2–4]. A further advance is implantation of electromagnetic beacons, the position of which can be detected in real-time during the treatment session. The vast majority of treatments with implanted electromagnetic beacons has occurred in prostate treatments; however, recent work has investigated their role in other treatment sites such as lung [5,6].

One of the benefits of implanted fiducial markers or electromagnetic beacons for targeting is the potential for real-time position information through continuous imaging, or electromagnetic signal read-out. Such real-time positional information can facilitate gating of the beam when the position of the target moves out of a pre-defined location, or real-time tracking of the target during the treatment [3,7–9]. Where the marker is implanted directly into the target, such as prostate, the accuracy of the surrogate is high. In the lung, however, there is limited opportunity to implant the marker directly into the tumor; implantation can be performed percutaneously, which carries a risk of pneumothorax, or endobronchially [4,10–14]. In the latter scenario, the implantation is constrained to parts of the lung or target that can be accessed through the bronchial tree. The result is that the markers are typically not implanted into the tumor, but into the surrounding parenchyma, potentially influencing the accuracy of the surrogate for tumor position [15–18]. The uncertainty may be confounded due to the complexity of lung motion with physiology such as respiration and the cardiac cycle, and with clinical conditions including fibrotic or emphysematous tissue [16,19–21].

In the current study, we analyze the accuracy of using electromagnetic beacons implanted endobronchially as surrogates for lung tumor motion. This is one component of the total geometric uncertainty in managing respiratory motion with the use of fiducial markers, known as surrogacy uncertainty [22]. We define surrogacy uncertainty (SU) as the variation in position between fiducial marker-indicated position and tumor position, at given time during treatment delivery. We use two methods of determining SU, 4DCT and fluoroscopic kilovoltage imaging, to quantify the SU for patients treated with real-time MLC tracking lung Stereotactic Ablative Body Radiotherapy (SABR).

Materials and Methods

Patients receiving SABR for early stage non-small cell lung cancer (NSCLC) or lung metastases who received MLC tracking treatment in the ethics approved LIGHT SABR trial (NCT02514512) were included in this study. This was a feasibility trial and included any patient receiving SABR to a primary lung lesion or lung metastasis. Each patient had three lung electromagnetic beacons (Calypso, Varian Medical Systems, Palo Alto, CA) implanted endobronchially under fluoroscopic guidance [5,23]. The lung specific beacons incorporated the electromagnetic beacons along with three prongs, which were embedded into the airway wall during insertion to minimize migration. Planning for implantation was performed using a pre-implant CT scan with the aim that all beacons were inserted as close as possible to the tumor, while attempting to form a triangle in three dimensions around the tumor. Each patient was prescribed either 48 Gy in 4 fractions (peripherally located tumor) or 50 Gy in 5 fractions (centrally located tumor). Two 6 MV ipsi-lateral VMAT arcs were used for all patients. Patients were treated with MLC tracking. Patient setup was performed by aligning the patient such that the centroid of the three implanted beacons was at the linac isocenter at end-exhale. Due to variations between respiratory cycles, the exact position of the centroid varied slightly at each end-exhale; however, since MLC tracking was in use, this variation was accounted for with MLC position. A free-breathing 3D cone beam CT was then acquired, to verify the relationship between the beacons and the tumor was consistent with that at time of simulation CT.

Imaging and Analysis

In the present analysis, the end-exhale phase of the breathing cycle was selected as the reference geometry as this is the treatment planning reference phase. The difference between the surrogate (centroid of the three markers) and the tumor center of mass (C.O.M) at each measurement time point was measured, and the distribution of these differences analyzed. Figure 1 is a schematic of the imaging and analysis described in the following sections.

4DCT Measurement

At least 7 days post-implant, a treatment planning 4DCT was acquired on a Philips BigBore CT scanner (Philips Healthcare, Eindhoven, The Netherlands). This was acquired in free breathing, and phase binning was performed based on the respiratory trace acquired from the Varian Real-time Position Management (RPM) system (Varian Medical Systems, Palo Alto, CA). The 4DCT was acquired with visual feedback for 7 patients for whom it was deemed to improve regularity of breathing, and this same feedback was used at treatment sessions. For the remaining patients visual feedback did not improve breathing regularity at 4DCT, and therefore no feedback was used at treatment.

The reconstructed slice thickness was 1.5 mm and in-plane dimensions were 1.2 mm x 1.2 mm. Ten phases were reconstructed. The tumor was contoured on each phase of the 4DCT by the treating radiation oncologist. The beacons were also contoured on each phase of the respiratory cycle.

For the 4DCT measurements, the position of each beacon, the centroid of the beacons and the tumor C.O.M relative to their positions at end-exhale phase was computed. The difference in the position of the centroid of the beacons relative to the position of the tumor C.O.M in each phase of the breathing cycle (4DCT) was computed and defined as the 4DCT SU (SU_{4DCT}). $SU_{4DCT,i}$ was calculated for each phase (i) of the 4DCT, where b_i is the beacon centroid position, b_{ex} is the beacon centroid position at end-exhale, t_i is the tumor C.O.M, and t_{ex} is the tumor C.O.M at end-exhale.

$$SU_{4DCT,\,i} = (b_{4DCT,i} - b_{4DCT,ex}) - (t_{4DCT,i} - t_{4DCT,ex})$$

Fluoroscopy Measurement

Following setup of the patient using the Calypso system and CBCT as previously described, and prior to treatment delivery at each fraction, including a mock-up fraction (Fx0), lateral and frontal fluoroscopy was acquired of the region encompassing all three beacons and the tumor. The kV field of view (FoV) was set to acquire an image at least 20 mm beyond the furthest extent of the beacons and tumor in each direction, and fluoroscopy was acquired for at least 2-3 breaths with 125 kV, 13 mAs and 10 frames per second. A set of frames is defined as all frames from a given angle in a fraction. On the first frame of each fluoroscopy set, each beacon was contoured, and these contours were then copied to each subsequent frame in the set. The tumor, or part of the tumor, if visible, was contoured on the first frame of the fluoroscopy set. The projected GTV contour from a digitally reconstructed radiograph from the treatment planning system was used as reference. The GTV contour was copied to each subsequent frame, and its position moved to match the tumor position in that frame. If the tumor was not visible, this set of frames was excluded from the analysis. Due to the subjective nature of tumor position measurement on the fluoroscopy frames, this was performed independently by two observers (Observer 1 & Observer 2). The root mean square error (RMSE) between the two observers for the centroid of the beacons and the tumor was computed per patient, over all analyzed frames.

The exhale frames were defined as the frames containing the superior most position of the beacon centroid in each respiratory cycle. The centroid of the beacons and the tumor C.O.M were determined in each exhale frame. The average exhale position of the centroid of the beacons was computed as $\bar{b}_{fluoro,ex}$, and of the tumor exhale positions as $\bar{t}_{fluoro,ex}$, over all respiratory cycles in that set of frames. In each frame (j) the SU in that frame, $SU_{fluoro,j}$, was computed as:

$$SU_{fluoro,\,j} = (b_{fluoro,\,j} - \overline{b}_{fluoro,\,ex}) - (t_{fluoro,j} - \overline{t}_{fluoro,ex})$$

Statistical analysis

Where SU_{fluoro} results are presented, this is the average of the two observers. Unless otherwise stated, the SU is presented by the 95th percentile for the SU_{4DCT} or SU_{fluoro}, computed over all frames or phases analyzed in each image set. That is, the data is ordered and the upper and lower 95% of the values are computed and presented as 5%/95% describing the upper and lower bounds of the distribution. In the case of SU_{4DCT} this represents the maximum out of the 10 phases. To determine any correlation of SU with beacon motion or distance of the beacons from the tumor, we computed the Pearson correlation coefficient and estimated the slope and associated 95% confidence interval of the relationships.

Results

The LIGHT SABR trial recruited 17 patients who were treated with MLC tracking to lung tumors. Of these, all 17 were available for the 4DCT analysis. The mean (range) tumor motion amplitude in the 4DCT scan was 5.9 mm (1.7 – 11.7 mm) in the SI direction, 2.2 mm (0.9 – 5.5 mm) in the LR direction, and 3.9 mm (1.2 – 12.9 mm) in the AP direction. For the fluoroscopy analysis, not all angles were acquired for all fractions due to time and patient comfort constraints. Moreover, on some fluoroscopy projections the tumor was not visible, and therefore could not be contoured. An average of 76 frames were acquired per projection angle (range 31-171). Due to the acquisition of two projection angles in most cases, two measurements in the SI direction of motion were acquired. Except where otherwise stated, we have combined SI measurement from the two projection angles. Supplementary Table 1 details the extent of the fluoroscopy data available for analysis.

Figure 2 shows the RMSE for the beacon and tumor position from two observers. There was minimal inter-observer variation in the beacon centroid position as identified on the fluoroscopy frames; where the average ± standard deviation (SD) RMSE in beacon segmentation was 0.2 ± 0.1 mm (SI), 0.1 ± 0.0 mm (LR) and 0.1 ± 0.1 mm (AP) for the three planes of motion over all patients (Figure 2a). The inter-observer variation in tumor position was larger; the average ± SD RMSE was 0.8 ± 0.5 mm (SI), 0.5 ± 0.2 mm (LR) and 0.7 ± 0.4 mm (AP) for the three planes of motion over all patients. The larger inter-observer differences in tumor segmentation (Figure 2b) compared with the beacons (Figure 2a) are likely due to the poorer visibility of the tumor on the fluoroscopy projections.

Figure 3 shows the probability distribution function (PDF) of the SU across all patients for the 4DCT and all fractions where fluoroscopy was obtained. There is an approximately symmetric distribution centered on

approximately zero in all planes, indicating that across the patients, the beacon motion either under or over-estimated the tumor motion. The maximum surrogacy uncertainties were 3.9 mm (SI), 3.6 mm (LR) and 6.5 mm (AP) as measured by 4DCT; and 4.1 mm (SI), 3.0 mm (LR) and 4.4 mm (AP) as measured by fluoroscopy. The 5th and 95th percentile were within 2.5 mm for all directions. **Error! Reference source not found.** summarizes the 5th and 95th percentile of the data presented in Figure 3. Supplementary Figure 1 provides individual patient distributions of SU for pre-treatment imaging (4DCT and mock up fraction) and during treatment imaging (fractions 1-5). Figure 4 plots the dominant SU_{fluoro} (either under or over estimation of tumor motion) represented by the maximum out of the 5th and 95th percentile of the SU_{fluoro} against the SU_{4DCT}; there was no correlation between the two measurements. A further comparison of the lateral and frontal fluoroscopy results is provided in the supplementary material.

Figure 5a & c shows the SU_{fluoro} of the individual beacons and beacon centroid in each direction as a function of the beacon or beacon centroid peak-to-peak motion in that direction. Figure 5b & d show the SU_{fluoro} for individual beacon and beacon C.O.M as a function of beacon-tumor distance. Table 2 describes the slopes of the lines of best fit to the data in Figure 5, and corresponding Pearson correlation coefficients. SU_{fluoro} is shown to increase with beacon motion for all three directions of motion. There was a weak correlation of the SU_{fluoro} for individual beacons or beacon centroids with the distance from the tumor, despite implantation of some beacons up to 95 mm from the center of the tumor. Similarly, Supplementary Figure 3 shows the dependence of SU_{4DCT} on peak-to-peak beacon motion and distance from tumor for both individual beacons and the centroid of all beacons. Figure 6 shows that when using the centroid of the three beacons, as opposed to individual beacons, there was a reduction in the SU_{fluoro} for some patients. The SU_{fluoro} (mean ± SD) reduced from: 2.0 ± 0.9 mm for individual beacons to 1.8 ± 0.8 mm for the beacon centroid in the SI direction; 1.3 ± 0.6 mm for individual beacons to 1.2 ± 0.6 mm for the beacon centroid in the LR direction; and 1.6 ± 0.8 mm for individual beacons to 1.4 ± 0.8 mm for the beacon centroid in the AP direction. This indicates that use of multiple beacons may be useful in reduction of surrogacy uncertainties. Using the slope of the SU_{fluoro} from the centroid of the three markers as a function of peak-to-peak beacon motion, the mean (95% CI) SU_{fluoro} was 5% (2% – 8%) of the motion magnitude in the SI direction, 16% (6% – 26%) of the motion magnitude in the LR direction and 33% (23% – 42%) of the magnitude in the AP direction.

Discussion

We have used pre-treatment volumetric and planar imaging to measure SU with the use of implanted markers as surrogates for tumor motion in lung SABR. In the current analysis endobronchially implanted electromagnetic beacons exhibited patient-specific geometric uncertainties when used as surrogates for

tumor motion. Various markers implanted endobronchially may have different anchoring mechanisms and subsequent migration risk. We have assessed the SU based on the position of the markers relative to the tumor at the time of simulation and treatment; therefore, the results obtained in this study would be applicable to any endobronchially implanted lung marker.

We observed increasing SU with increasing motion, increased SU in the SI direction, and by definition of SU, increased SU in the inhale phases. This is in agreement with that observed in other studies based on both fluoroscopy and 4DCT measurements [15,24]. The dependence on tumor motion suggests that a larger margin may be required for patients with large excursion. The magnitude of these uncertainties approached half of the tumor motion when motion was low. This has implications for the use of implanted markers as surrogates of tumor position or motion depending on the motion management strategy employed. For real-time tracking, the SU as a function of motion magnitude indicates a lower threshold below which the uncertainties introduced by use of a surrogate for tumor motion approaches the magnitude of tumor motion, therefore, clinical benefit may be limited. In contrast, in a respiratory gating scenario in which the beam is only turned on when the surrogate is in a given position, the impact of SU may be reduced [15].

A number of previous studies have evaluated the SU as a function of marker distance from the tumor, and in general show increasing SU with increasing distance from the tumor [15–18]. However, these studies show large variability between patients, and between locations within the lobe, showing that in some instances, markers implanted at relatively large distances from the tumor could still represent tumor motion [18]. Figure 5b shows that the majority of our markers were within 50 mm of the tumor, and only 3 markers were greater than 70 mm from the tumor. The SU_{fluoro} for one of these markers was over 4 mm in the SI direction; however, for the two markers at more than 80 mm from the tumor, the SU_{fluoro} was below 3 mm in all directions. This was likely not influenced by low motion amplitude; the mean (range) of motion of markers > 70 mm from the tumor was 5.8 mm (3.2 – 13.3 mm) in the SI direction, 1.5 mm (1.3 – 1.7 mm) in the LR direction and 2.4 mm (0.6 – 5.3 mm) in the AP direction, which is slightly lower than the mean (range) of motion of markers < 70 mm from the tumor: 8.4 mm (0.6 – 18.9 mm) in the SI direction , 2.7 mm (0.6 – 7.2 mm) in the LR direction and 3.5 mm (0.6 – 8.2 mm) in the AP direction.

There was reduction in SU when using the centroid of multiple beacons as the surrogate of tumor motion compared with individual beacon motion; however, this was patient and beacon specific. This is in agreement with Lizuka et al. who observed similar results, showing combinations of markers provided the most accurate surrogate for tumor motion, based on 4DCTs with a 320-slice CT scanner [16]. In four

patients, a single marker was removed from the tracking algorithm for treatment as it did not represent tumor motion as visualized on the treatment planning 4DCT. This indicates that when using endobronchially inserted markers that are not implanted directly into the tumor, the use of multiple beacons potentially provides robustness to uncertainty in tracking objects using a surrogate. This applies to any real-time tracking based on implanted surrogates, such as the CyberKnife Synchrony system, gimbal-based systems or MLC tracking.

The lack of correlation between the SU as measured by the 4DCT and that as measured with fluoroscopy highlights the impact of the various uncertainties in the measurement process. In the 4DCT acquisition, each anatomical slice of approximately the collimation width (24 mm) is imaged for about one breath; therefore, we are able to measure SU from peak inhale to peak exhale for one breath. Moreover if the beacons and tumor span more than this distance, then the motion observed in the 4DCT is from different breaths. This will introduce uncertainty when there are breathing variations, as the SU would then be due to breathing variation, in addition to true displacement variation. This limitation may be overcome through use of volumetric imaging encompassing all markers and the tumor [16]. Further, in the intermediate phases of the 4DCT, rapid motion of the beacons and tumor result in artefacts in the image which limit the accuracy to which the objects can be delineated. Supplementary Figure 1 shows two cases with large AP SU_{4DCT}. These two cases had significant artefacts in the 4DCT due to irregular breathing during acquisition, which impacted the SU_{4DCT} measurement. In the fluoroscopy acquisition, higher temporal and spatial resolution is achieved, and multiple breaths can be imaged. Importantly, by imaging with a FoV encompassing all three beacons and the tumor, SU is calculated on the same breaths between the beacons and the tumor. The improvements in spatial and temporal resolution come at the expense of reduced soft-tissue contrast in the fluoroscopic imaging. This limits the accuracy to which the tumor motion can be determined. We have measured inter-observer tumor segmentation with two observers; for some patients, the estimated uncertainties from measurement of SU are of the same magnitude as the SU itself; we had up to a 2.5 mm RMSE between two observers for measurement of the tumor position based on fluoroscopy. Moreover, we observed low correlation between SU_{fluoro} as measured with either frontal or lateral projections, despite moderate correlation between observers for each of these projection angles (Supplementary Figure 2). The exact cause of this is unknown, but since the amplitude of respiratory motion was relatively consistent between projection angles suggesting consistent breathing traces, this may be related to visualization of the tumor between the two projection angles, relative to bone and other anatomy. Although there were specific patients with larger measured SU, on a population basis, from the 4DCT and both treatment and mock up fractions, the population 5^{th}/95^{th} percentiles were

up to -2.0 mm/2.1 mm. Therefore, we believe it is pragmatic to apply a population-based uncertainty estimate for the SU component of geometric uncertainty, rather than a patient specific margin to account for SU.

Conclusion

We have estimated the uncertainty in localizing lung tumors from use of bronchoscopically implanted electromagnetic beacons using 4DCTs and pre-treatment fluoroscopy imaging. The surrogacy uncertainty on a population basis was symmetric about zero, with a 95th percentile up to 2.3 mm. There was a weak dependence on motion magnitude, but no dependence on distance of implanted beacon from tumor. It is recommended that population-based margins be used to account for this component of geometric uncertainty.

References

1. Jaffray DA, Langen KM, Mageras G, et al. Safety considerations for IGRT: Executive summary. *Pract Radiat Oncol*. 2013;3(3):167-170. doi:10.1016/j.prro.2013.01.004

2. Nuyttens JJ, Prévost JB, Praag J, et al. Lung tumor tracking during stereotactic radiotherapy treatment with the CyberKnife: Marker placement and early results. In: *Acta Oncologica*. Vol 45. ; 2006:961-965. doi:10.1080/02841860600902205

3. Harada T, Shirato H, Ogura S, et al. Real-time tumor-tracking radiation therapy for lung carcinoma by the aid of insertion of a gold marker using bronchofiberscopy. *Cancer*. 2002;95(8):1720-1727. doi:10.1002/cncr.10856

4. Kupelian PA, Forbes A, Willoughby TR, et al. Implantation and Stability of Metallic Fiducials Within Pulmonary Lesions. *Int J Radiat Oncol Biol Phys*. 2007;69(3):777-785. doi:10.1016/j.ijrobp.2007.03.040

5. Dobelbower MC, Popple RA, Minnich DJ, et al. Anchored Transponder Guided Lung Radiation Therapy. *Pract Radiat Oncol*. 2020;10(1):e37-e44. doi:10.1016/j.prro.2019.08.009

6. Willoughby TR, Kupelian PA, Pouliot J, et al. Target localization and real-time tracking using the Calypso 4D localization system in patients with localized prostate cancer. *Int J Radiat Oncol Biol Phys*. 2006;65(2):528-534. doi:10.1016/j.ijrobp.2006.01.050

7. Booth JT, Caillet V, Hardcastle N, et al. The first patient treatment of electromagnetic-guided real

time adaptive radiotherapy using MLC tracking for lung SABR. *Radiother Oncol*. 2016;121(1):19-25. doi:10.1016/j.radonc.2016.08.025

8. Pepin EW, Wu H, Zhang Y, Lord B. Correlation and prediction uncertainties in the CyberKnife Synchrony respiratory tracking system. *Med Phys*. 2011;38(7):4036-4044. doi:10.1118/1.3596527

9. Ozhasoglu C, Saw CB, Chen H, et al. Synchrony - Cyberknife Respiratory Compensation Technology. *Med Dosim*. 2008;33(2):117-123. doi:10.1016/j.meddos.2008.02.004

10. Imura M, Yamazaki K, Shirato H, et al. Insertion and fixation of fiducial markers for setup and tracking of lung tumors in radiotherapy. *Int J Radiat Oncol Biol Phys*. 2005;63(5):1442-1447. doi:10.1016/j.ijrobp.2005.04.024

11. Hong JC, Yu Y, Rao AK, et al. High retention and safety of percutaneously implanted endovascular embolization coils as fiducial markers for image-guided stereotactic ablative radiotherapy of pulmonary tumors. *Int J Radiat Oncol Biol Phys*. 2011;81(1):85-90. doi:10.1016/j.ijrobp.2010.04.037

12. Jackson P, Steinfort DP, Kron T, Siva S. Practical assessment of bronchoscopically inserted fiducial markers for image guidance in stereotactic lung radiotherapy. *J Thorac Oncol*. 2016;11(8):1363-1368. doi:10.1016/j.jtho.2016.04.016

13. Nabavizadeh N, Zhang J, Elliott DA, et al. *Electromagnetic Navigational Bronchoscopy-Guided Fiducial Markers for Lung Stereotactic Body Radiation Therapy: Analysis of Safety, Feasibility, and Interfraction Stability*. Vol 21.; 2014. doi:10.1097/LBR.0000000000000065

14. Shah AP, Kupelian PA, Waghorn BJ, et al. Real-time tumor tracking in the lung using an electromagnetic tracking system. *Int J Radiat Oncol Biol Phys*. 2013;86(3):477-483. doi:10.1016/j.ijrobp.2012.12.030

15. Ueki N, Matsuo Y, Nakamura M, et al. Intra- and interfractional variations in geometric arrangement between lung tumours and implanted markers. *Radiother Oncol*. 2014;110(3):523-528. doi:10.1016/j.radonc.2014.01.014

16. Iizuka Y, Matsuo Y, Nakamura M, et al. Optimization of a newly defined target volume in fiducial marker-based dynamic tumor-tracking radiotherapy. *Phys Imaging Radiat Oncol*. 2017;4(June):1-5. doi:10.1016/j.phro.2017.10.001

17. Yamazaki R, Nishioka S, Date H, Shirato H, Koike T, Nishioka T. Investigation of the change in marker geometry during respiration motion: A preliminary study for dynamic-multi-leaf real-time tumor tracking. *Radiat Oncol*. 2012;7(1):1-5. doi:10.1186/1748-717X-7-218

18. Smith RL, Yang D, Lee A, Mayse ML, Low DA, Parikh PJ. The correlation of tissue motion within the lung: Implications on fiducial based treatments. *Med Phys*. 2011;38(11):5992-5997. doi:10.1118/1.3643028

19. Shah AP, Kupelian PA, Waghorn BJ, et al. Real-time tumor tracking in the lung using an electromagnetic tracking system. *Int J Radiat Oncol Biol Phys*. 2013;86(3):477-483. doi:10.1016/j.ijrobp.2012.12.030

20. Tong L, Laura IC, Xiaoli T, Nuno V, Steve BJ. Fluoroscopic tumor tracking for image-guided lung cancer radiotherapy. *Phys Med Biol*. 2009;54(4):981. http://stacks.iop.org/0031-9155/54/i=4/a=011.

21. Chen H, Zhong Z, Yang Y, et al. Internal Motion Estimation by Internal-external Motion Modeling for Lung Cancer Radiotherapy. *Sci Rep*. 2018;8(1). doi:10.1038/s41598-018-22023-3

22. Caillet V, Zwan B, Briggs A, et al. Geometric uncertainty analysis of MLC tracking for lung SABR. *Phys Med Biol*. August 2020. doi:10.1088/1361-6560/abb0c6

23. Jaccard M, Champion A, Dubouloz A, et al. Clinical experience with lung-specific electromagnetic transponders for real-time tumor tracking in lung stereotactic body radiotherapy. *Phys Imaging Radiat Oncol*. 2019;12:30-37. doi:10.1016/j.phro.2019.11.002

24. Nakamura M, Takamiya M, Akimoto M, et al. Target localization errors from fiducial markers implanted around a lung tumor for dynamic tumor tracking. *Phys Medica*. 2015;31(8):934-941. doi:10.1016/j.ejmp.2015.06.012

Figure Captions

Figure 1: Schematic of the imaging and analysis process. 4DCT and fluoroscopy imaging was acquired. The surrogates for tumor motion and the tumor were identified on each temporal phase or frame. These positions were then normalized to the exhale position (average exhale position on fluoroscopy shown as red line). The distribution of the differences between the surrogate and tumor was then analyzed. The red triangles indicate the 5th and 95th percentile for this example distribution, and the red line the mean.

Figure 2: Agreement between the two observers for (a) the surrogate (centroid of three beacons) and (b) the tumor, as measured with fluoroscopy. The inter-observer RMSE of the tumor or beacon location is presented for each patient, in each anatomical direction (SI, LR and AP). The median and mean values are represented as a circle and a cross, respectively.

Figure 3: Box plots (left panel) and PDFs (right panel) of the SU as measured by 4DCT and fluoroscopy for (a) SI, (b) LR (frontal) and (c) AP (Lateral). The box indicates the middle 50% of the data, while the whiskers indicate the 5th and 95th percentiles. The median and mean of each distribution are represented by a horizontal line and a cross, respectively. The SU PDFs have uniform bin size of 0.5 mm, while the triangles on the y-axis represent the 5th and 95th percentiles (i.e. mirror the box whiskers). The SI from both frontal and lateral projections has been combined.

Figure 4: Maximum out of the 5th or 95th percentile values of the SU_{fluoro} compared with SU_{4DCT}, with corresponding Pearson correlation coefficients (r).

Figure 5: SU_{fluoro} (95th percentile): (a) individual beacon and (c) beacon centroid SU_{fluoro} as a function of peak-to-peak motion of the individual beacon or beacon centroid; (b) individual beacon and (d) beacon centroid SU_{fluoro} as a function of 3D vector distance from the tumor. The shaded area corresponds to the 95% confidence interval of the estimated slope (solid line) in each direction.

Figure 6: Average SU_{fluoro} (95th percentile) across all directions, calculated for all individual beacons (blue) and the centroid of the three beacons (red). The error bar is equal to +/- 1 standard deviation.

Table 1: 5th and 95th percentile SU over the population as measured on the 4DCTs and fluoroscopy data. The data for each individual projection angle is provided for fluoroscopy.

Source	SI (Lateral, mm)	SI (Frontal, mm)	LR (mm)	AP (mm)
4DCT	[-1.9, 1.8]	[-1.9, 1.8]	[-2.0, 1.2]	[-2.0, 2.1]
Fluoro [Fx0-5]	[-2.3, 1.3]	[-1.7, 0.9]	[-1.5, 1.2]	[-1.9, 1.0]

Table 2: 95th percentile SU_{fluoro} as a function of peak-to-peak motion and distance from tumor for individual beacons and C.O.M of three beacons.

95th Percentile SU_{fluoro} vs.	Projection	Slope		Pearson Correlation Coefficient		
		Value	95% CI	Value	95% CI	p-value
Peak-to-Peak Beacon Motion (Individual Beacons)	**SI**	0.07	0.04 – 0.09	0.35	0.24 – 0.46	0.0000
	LR	0.15	0.08 – 0.21	0.39	0.23 – 0.53	0.0000
	AP	0.25	0.14 – 0.35	0.42	0.25 – 0.57	0.0000
Peak-to-Peak Beacon Motion (Beacons centroid)	**SI**	0.05	0.02 – 0.08	0.33	0.13 – 0.51	0.0021
	LR	0.16	0.06 – 0.26	0.45	0.18 – 0.65	0.0016
	AP	0.33	0.23 - 0.42	0.76	0.58 – 0.87	0.0000
Distance to Tumor (Individual Beacons)	**SI**	0.02	0.01 – 0.02	0.28	0.16 – 0.39	0.0000
	LR	0.01	0.00 – 0.01	0.20	0.03 – 0.36	0.0249
	AP	0.00	-0.01 – 0.01	-0.08	-0.27 – 0.11	0.3808
Distance to Tumor (Beacons centroid)	**SI**	0.01	-0.01 – 0.02	0.11	-0.10 – 0.32	0.3069
	LR	0.02	0.01 – 0.04	0.41	0.14 – 0.63	0.0039

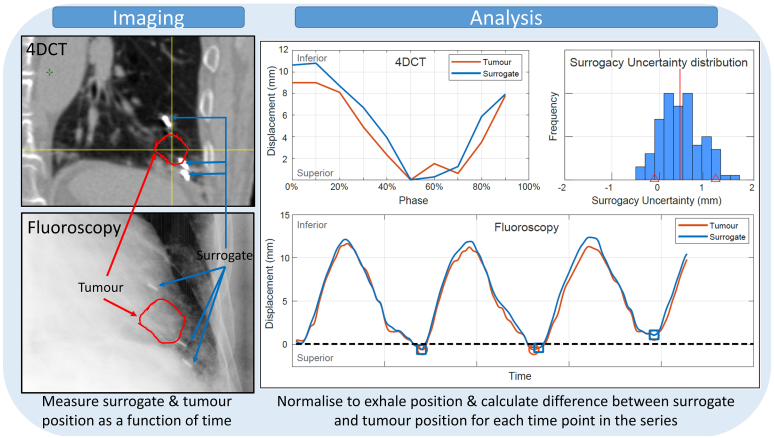

mp_14788_f1.tif

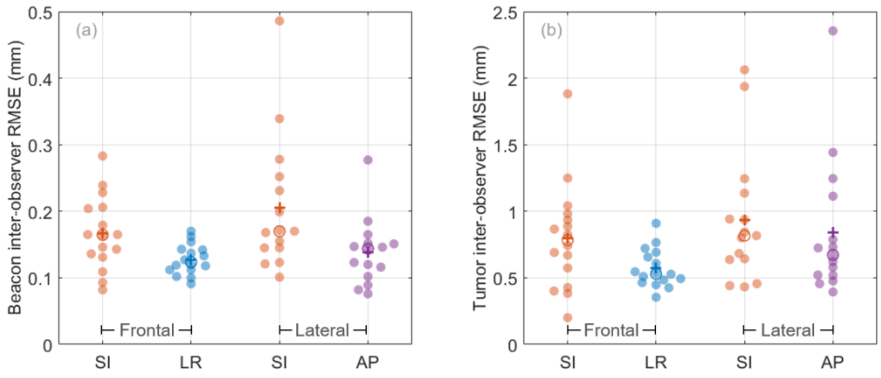

mp_14788_f2.tif

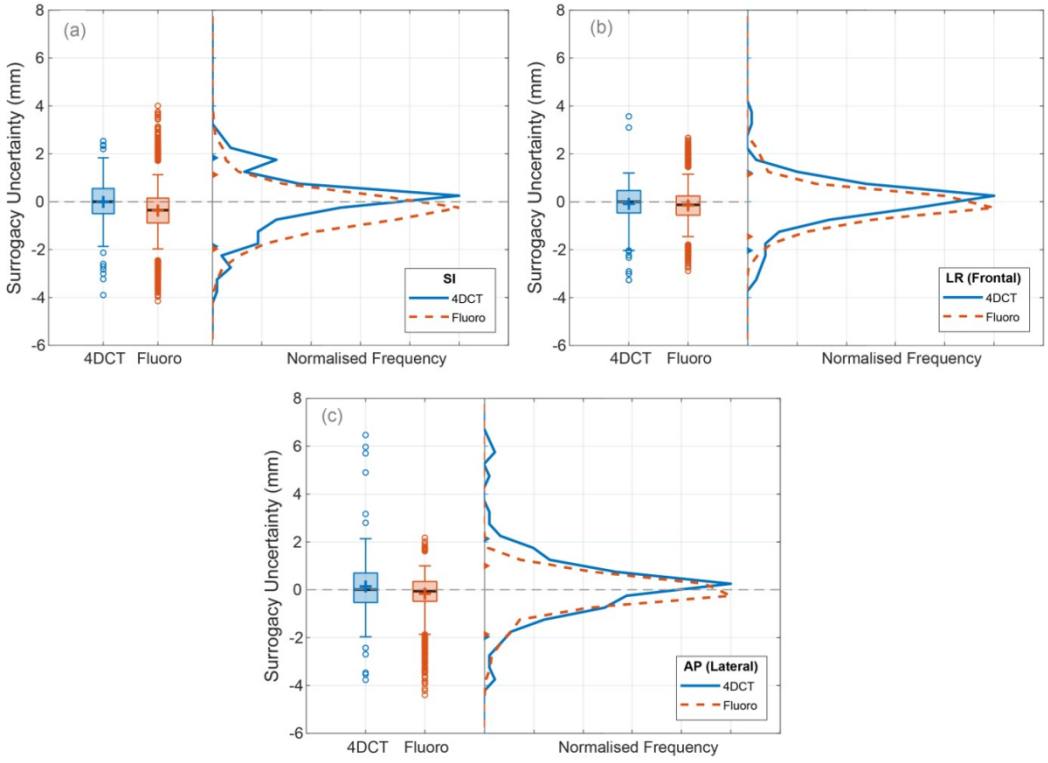

mp_14788_f3.tif

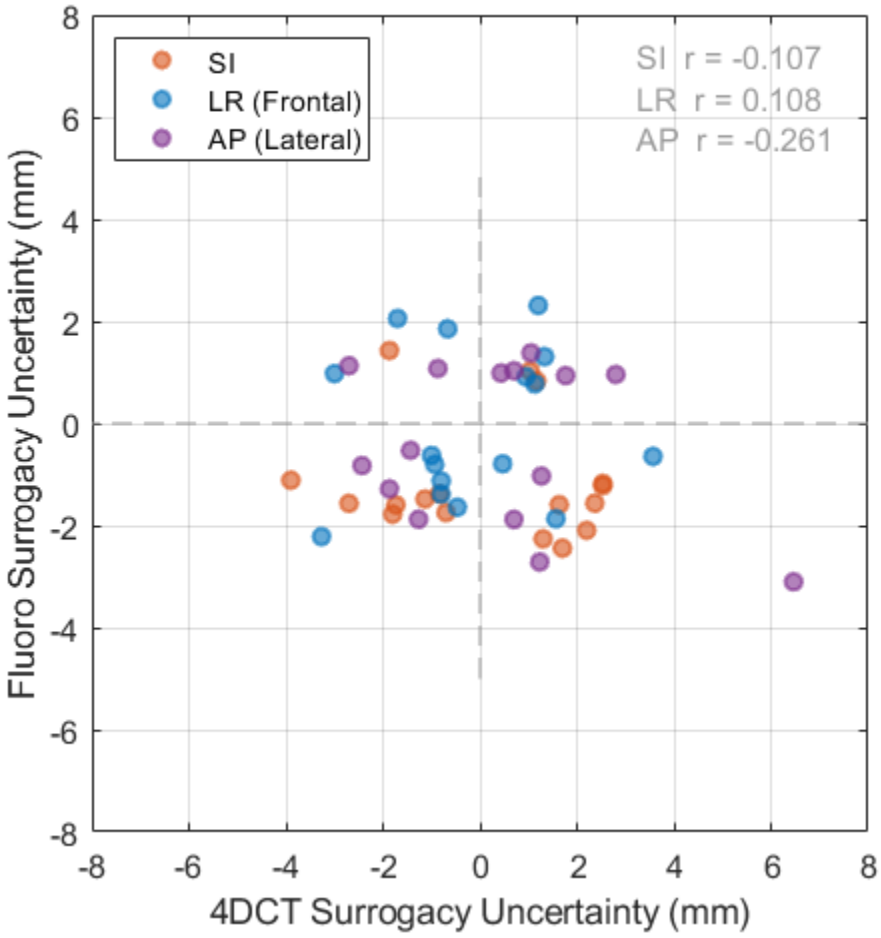

mp_14788_f4.tif

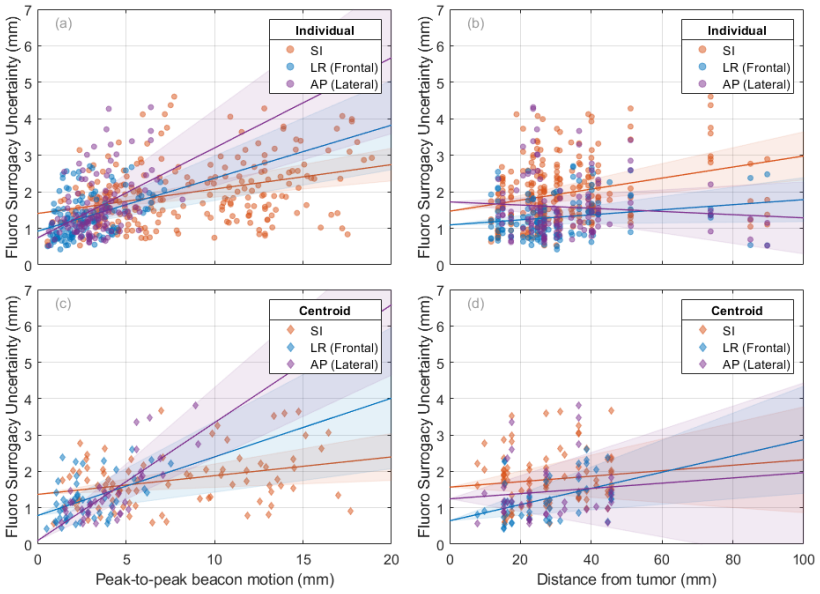

mp_14788_f5.tif

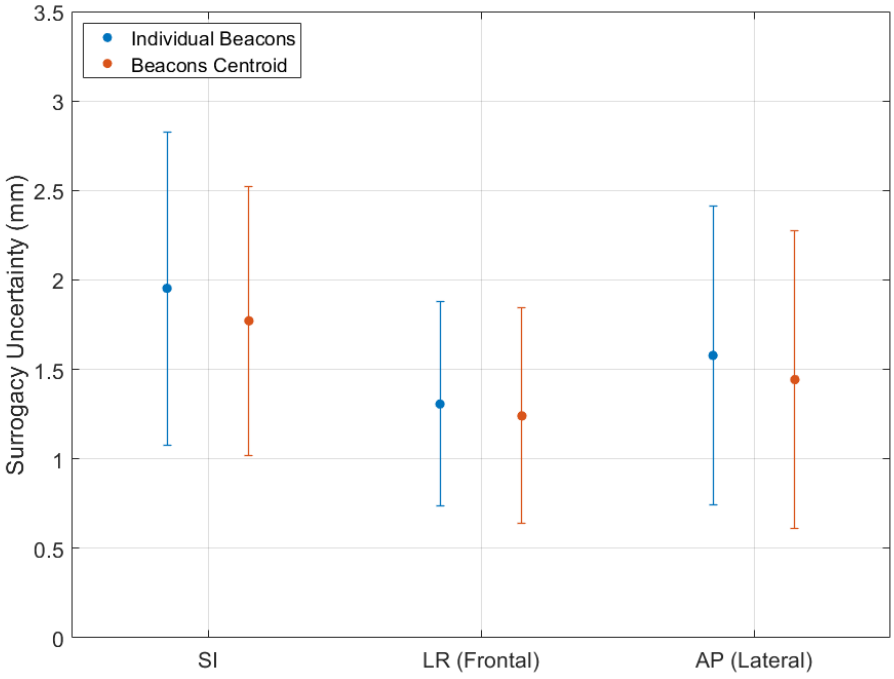

mp_14788_f6.tif